Development of reflection gratings for advanced ECRH scenarios

Burkhard Plaum[1,*], *Martin* Schubert[2], *Achim* Zeitler[1], *Walter* Kasparek[1], *Carsten* Lechte[1], *Jörg* Stober[2] and ASDEX Upgrade Team[2]

[1]Institut für Grenzflächenverfahrenstechnik und Plasmatechnologie, Universität Stuttgart, Pfaffenwaldring 31, D-70569 Stuttgart, Germany
[2]Max-Planck-Institut für Plasmaphysik, Boltzmannstr.2, D-85748 Garching, Germany

Abstract. An existing framework for the design of reflection gratings was reworked. It takes the astigmatic complex beam parameters and the orientations of the beam axes of the incident and reflected beams as input and synthesizes a grating, which transforms the incident beam into the reflected beam. This is done by decomposing the 3D problem into a series of 2D reflections of plane waves. The 2D grating profiles are optimized in parallel on multiple computers. Finally, the 3D grating is derived using a simplified interpolation scheme.

1 Introduction

When heating fusion plasmas at higher harmonics of the electron cyclotron frequency, the absorption efficiency can be reduced. This leads to a significant transmitted beam power hitting the wall at the high field side (HFS). To protect the wall and to use the remaining power, one method is to place a specialized reflector at the HFS, which directs the beam back into the plasma for a second heating pass [1]. The reflector needs to conform to the tiles at the HFS, which are often non-planar. The direction of the reflected beam is chosen such that the absorption of the second heating pass is maximized and the wall area at the LFS, which is hit after the second pass, contains no sensitive components. Additional requirements are a refocusing of the beam and polarization independence of the reflection characteristics. All these conditions can only be fulfilled with a grating. The design process involves the decomposition of the 3D field problem into a series of 2D reflections of plane waves. After the 2D gratings are optimized, the final 3D grating is synthesized.

2 Design process

For the definition of the problem the astigmatic beam parameters of the incident and reflected Gaussian beams are required as well as the orientations of the beam axes. These are obtained by a series of beam tracing simulations using the TORBEAM code [2]. These runs are done for different typical heating scenarios and the most appropriate beam parameters are obtained by averaging [3]. Furthermore the basic shape of the reflector is needed. In the case of the high field side of a tokamak, it is a saddle-type shape defined by the curvature radii in the toroidal and poloidal directions. In local coordinates of the reflector, the shape is given in terms of the surface height $z(x,y)$ and the orientation of the normal vector $\mathbf{n}(x,y)$. Using these parameters, we can calculate the local wave vectors $\mathbf{k}_{in}(x,y)$ and $\mathbf{k}_{out}(x,y)$.

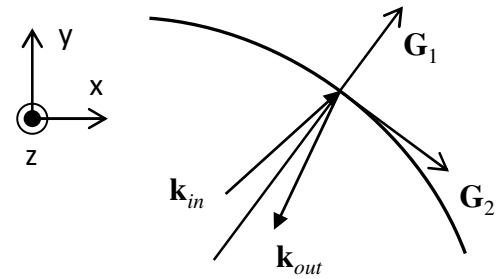

Fig. 1. Local k vectors and the resulting grating vectors (top view)

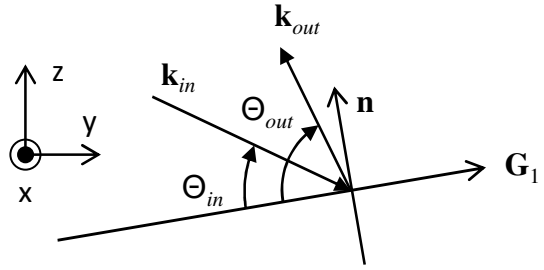

Fig. 2 Local k vectors (side view)

Figures 1 and 2 show the definition of the grating vectors. $\mathbf{G}_1$ is tangential to the surface and lies in the middle plane between $\mathbf{k}_{in}$ and $\mathbf{k}_{out}$. $\mathbf{G}_2$ is perpendicular to the middle plane and defines the direction of the groove. Parallel to the groove we have a reflection according to

* Corresponding author: plaum@igvp.uni-stuttgart.de

the reflection law (Fig. 1). Perpendicular to the groove we have the angles Θ_{in} and Θ_{out}, which, together with the diffraction order n, completely define one local 2D problem.

From an arbitrary start point and by using the known grating period, we can obtain a discretized form of the groove layout by integrating $\mathbf{G}_1$ with a standard Runge-Kutta method. An example is shown in Fig. 3.

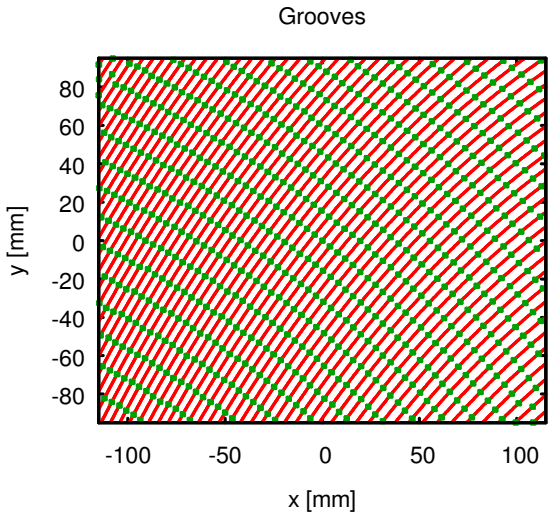

Fig. 3 Groove layout (red lines) and optimization points (green dots) for the 2D profiles

We now define the points, for which 2D gratings will be optimized. The distance of two neighboring points along the grooves is defined by the differences of the angles Θ_{in} and Θ_{out}:

$$|\Delta\theta_{in}| + |\Delta\theta_{out}| = 1° \qquad (1)$$

Depending on the actual beam parameters, this can result in a large (≈1000) number of 2D profiles (green dots in Fig. 3). This number can be reduced by quantizing the values for Θ_{in} and Θ_{out}: If the angles are rounded e.g. to a resolution of 0.5°, a number of 2D gratings become identical and need to be optimized just once. Fig. 4 shows the number of distinct profiles as a function of the angular resolution. While the actual numbers can change strongly depending on the actual beam configuration, the reduction rate is always significant. Earlier works [4] showed that angular errors of up to 1° are acceptable. The angular resolution is a simple parameter for finding a compromise of accuracy and optimization time.

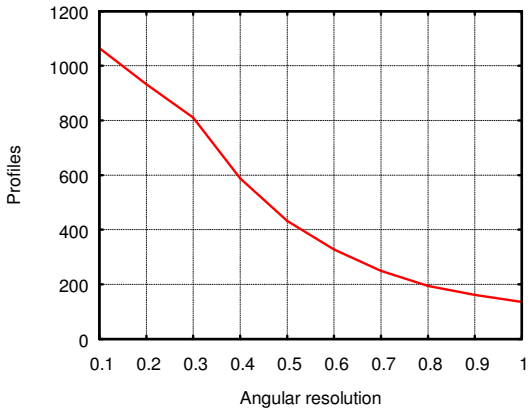

Fig. 4 Number of distinct profiles as a function of the angular resolution

The optimization goal for the 2D profiles is a maximum power in the desired diffraction order and minimum phase difference between the polarizations. The cost function is defined in terms of an efficiency η:

$$\eta = \frac{1}{4} I_n^{TE} + \frac{1}{4} I_n^{TM} + \frac{1}{2}\sqrt{I_n^{TE} I_n^{TM}}\cos(\Phi_n^{TE,TM}) \qquad (2)$$

This results ideally in a focused reflected beam, which has the same elliptical polarization as the incident beam. Non-zero power in other diffraction orders will result in stray radiation. A non-zero phase difference will make the grating birefringent.

The profiles are modeled by Fourier series where the coefficients are the parameters for the optimizer. The DC-coefficient is not used for the optimization because it is not relevant for a plane wave reflection. Furthermore, a horizontal phase shift of the grating does not change the behavior because the BEM solver implicitly assumes an infinite periodicity of the 2D grating. Thus, we need only the cosine coefficient for the first order. The maximum order of coefficients is obtained from the wavelength and the sampling theorem. As a start value for the optimizer we use an Echelette grating.

The 2D profiles can be optimized on different CPUs on different computers simultaneously, because they are independent problems. For each 2D grating ten optimizations are run with different seeds for the random number generator. For the presented example, 5 Intel Xeon servers and one desktop PC with a total of 184 cores were running for 3 days.

Fig. 5 shows examples for optimized 2D profiles. After the optimization the profiles are shifted such that the maximum value (z = 0) is located at the boundaries. This ensures that no discontinuities can occur between adjacent grooves.

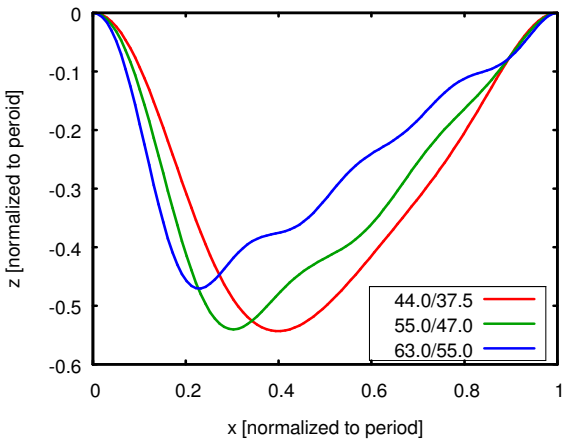

Fig. 5 Optimized 2D profiles for different combinations of Θ_{in} and Θ_{out}

The final grating is then calculated by interpolation of the 2D gratings. Fig. 6 shows the interpolation scheme. For a point (x,y) (cross in Fig. 6), we first identify the groove number.

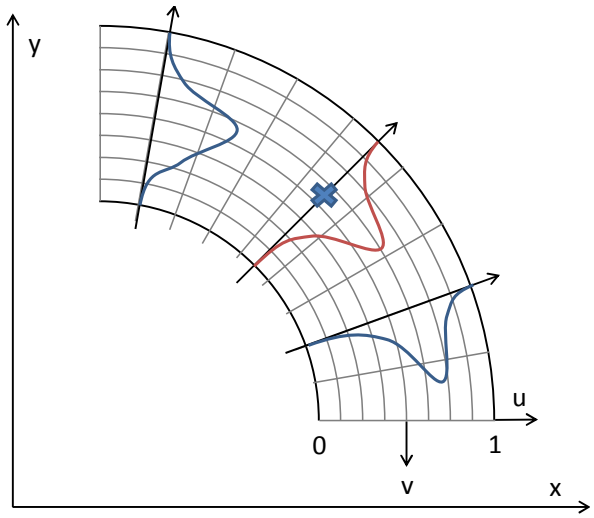

Fig. 6 Interpolation scheme for the final 3D grating. The cross is the point, for which the local z-coordinate is calculated. Note that in general the groove width is not constant.

Then, we transform the mirror coordinates x and y to groove-local coordinates u and v. The coordinate u corresponds to the grating vector $\mathbf{G}_1$ and is normalized to the grating period. The coordinate v corresponds to the vector $\mathbf{G}_2$ and is in metric units. We can now obtain a local groove profile linear interpolation of the two neighboring profiles. This interpolation is done for the Fourier coefficients along the coordinate v. Finally, the actual local z-coordinate of the grating is obtained with the interpolated Fourier coefficients and the u coordinate.

This interpolation scheme ensures a smooth surface without any discontinuities. Since the actual interpolation is done in one dimension, the method is also quite simple.

In summary, the reworked optimization framework has the following new features compared to the earlier code:

- Generic coordinates for the beam parameters. The original code was tightly coupled to ASDEX-Upgrade for the mirror positions and TORBEAM for the beam parameters. It was not directly usable in other environments.
- Parallelized optimization of the 2D gratings
- Adjustable angular resolution to reduce the number of distinct gratings. The original code worked with fixed 1° steps.
- Simple 1D interpolation for the final grating. The original code used a generic triangulation and subsequent 2D interpolation.
- New analysis- and visualization tools

3 Result

Fig. 7 shows the interpolated grating, which was designed for the ECRH system of ASDEX-Upgrade [5]. One can see the saddle type basic shape. The orientation and period of the grooves correspond to Fig. 3.

Fig. 8 shows the efficiencies according to (2) of the 2D profiles. One can see that the efficiency increases monotonically from left to right. In two regions however, it drops to lower values. The increasing behavior of the efficiency corresponds to the angles Θ_{in} and Θ_{out} (See Figs 9 and 10) where a steeper beam incidence results in better efficiencies. The abrupt drop of the efficiency is in agreement with Fig. 11, where the number of existing diffraction orders is plotted. If the number of orders increases, the optimization problem becomes more difficult, because it includes the suppression of all diffraction orders except the wanted one. Furthermore, Fig. 8 indirectly confirms the convergence of the optimizer. A poor convergence (i.e. when the optimizer gets stuck at sub-optimal results) would result in more noise in the efficiency plot.

For cases, where several tiles are possible candidates for an ECRH reflector, a plot of the diffraction orders like in Fig. 11 can be helpful. It always corresponds to the final efficiency but can be calculated quickly before doing the actual optimization.

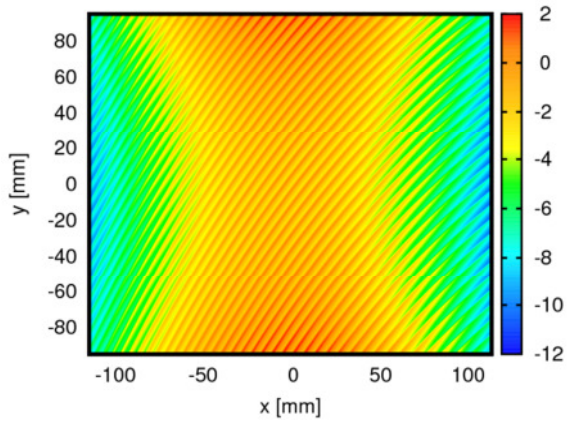

Fig. 7 Interpolated grating

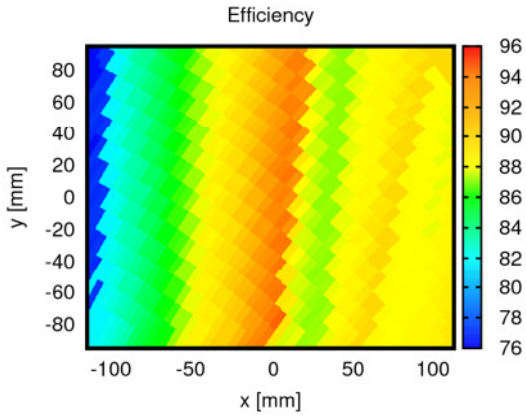

Fig. 8 Efficiency map of the grating

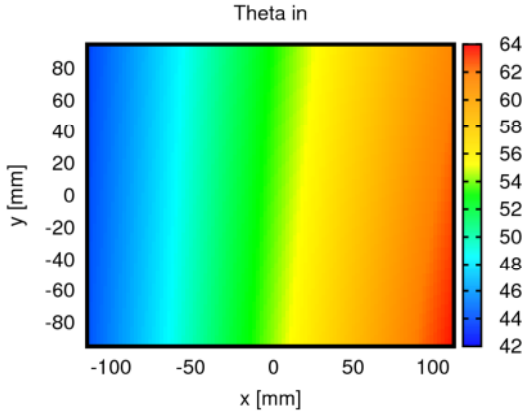

Fig. 9 Distribution of Θ_{in} on the grating

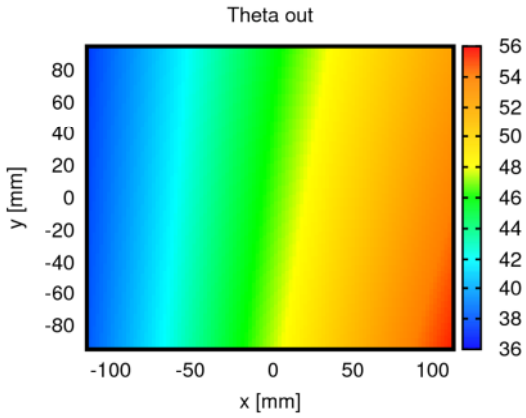

Fig. 10 Distribution of Θ_{out} on the grating

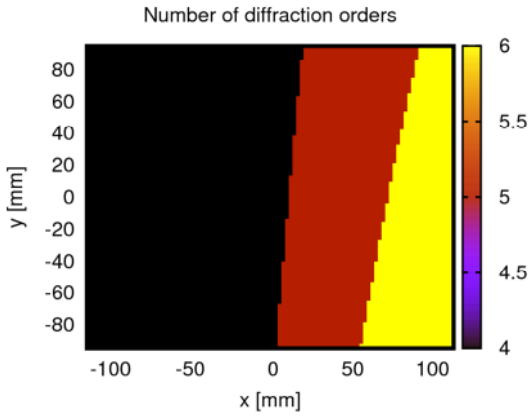

Fig. 11 Numbers of existing diffraction orders on the grating

4 Manufacturing

The reflector was manufactured from graphite with a numerical milling machine. An important issue is the selection of the milling cutter. The shape of the milling cutter limits the difference of the maximum and minimum slope angles on the grating. Typically, cylindrical cutters are preferred due to their robustness. However, they allow a maximum angle difference of 90°. The better choice is a dovetail cutter like in Fig. 12. It allows a maximum angle difference of e.g. 135°.

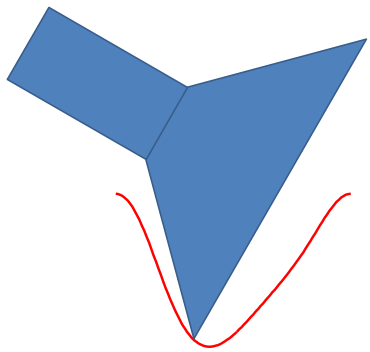

Fig. 12. Dovetail milling cutter for a slope angle difference of 135° in a typical groove profile.

The maximum allowed slope angle difference can be passed as a parameter to the optimizer. An example for

the influence of this parameter on the achieved efficiency is shown in Fig. 13.

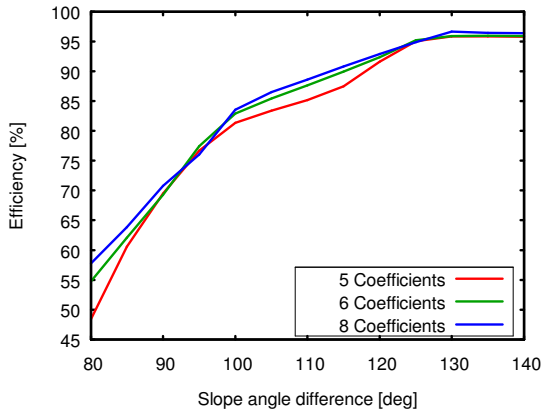

Fig. 13 Efficiency of an optimized 2D grating as a function of the allowed slope angle difference

One can see that for this example the limitation to 90° results in an efficiency below 70%, while for 135° it is above 95%. Also shown are the curves for different numbers of Fourier coefficients. According to the sampling theorem, 5 coefficients are sufficient for this example. We can see that increasing the number beyond 5 does not lead to significant improvements, especially if the 135° cutter is used. Fig. 14 shows the reflector in the milling machine.

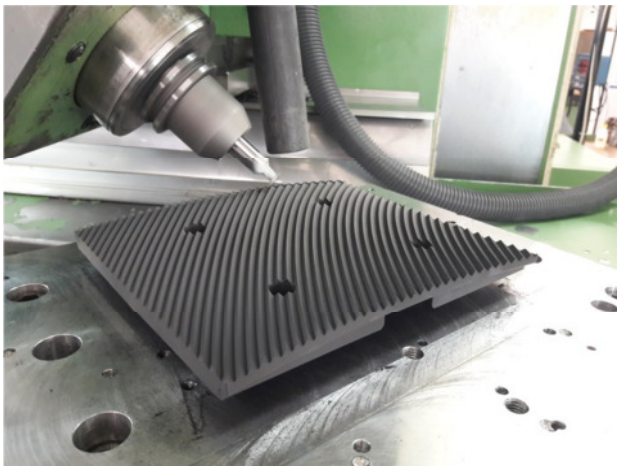

Fig. 14. Reflector in the milling machine

After milling the reflector was coated with a thin tungsten layer (13–15 µm) to become compatible with the ASDEX-Upgrade requirements.

5 Measurement

To characterize the reflector experimentally, a measurement was done with a vector network analyzer and an *x-y* scanner, Fig. 15 shows the setup. The reflector is mounted on a goniometer, which allows to arbitrary rotate the reflector (see Fig. 16). The incident beam was generated by a lens horn which produces a circular Gaussian beam. It is slightly different from the astigmatic beam used for the optimization. The important parameter, however, is the phase front curvature on the mirror, which is comparable in both directions.

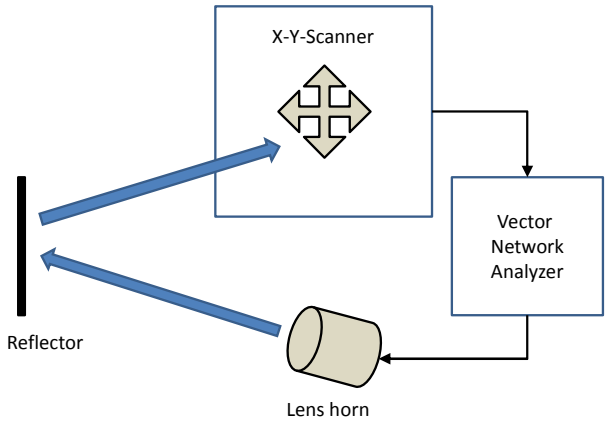

Fig. 15 Experimental setup

Fig. 16 Reflector mounted on a goniometer

The measured fields are shown in Figs 17 – 20. We can see a slightly elliptical beam with an astigmatic phase, which is similar to the design value. Also important is the similarity between the two polarizations, which was an optimization goal.

For a more detailed analysis it would be necessary to also measure the spurious fields due to unwanted diffraction orders. This would, however, require a field scan over a large solid angle, which is not possible with the current equipment.

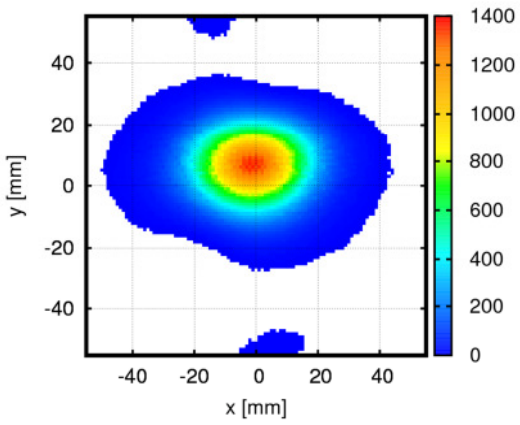

Fig. 17 Measured intensity for horizontal polarization

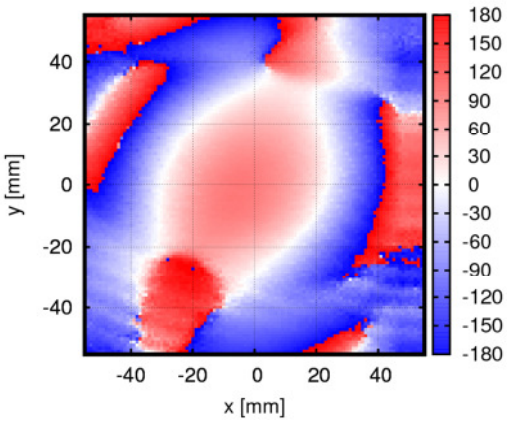

Fig. 18 Measured phase for horizontal polarization

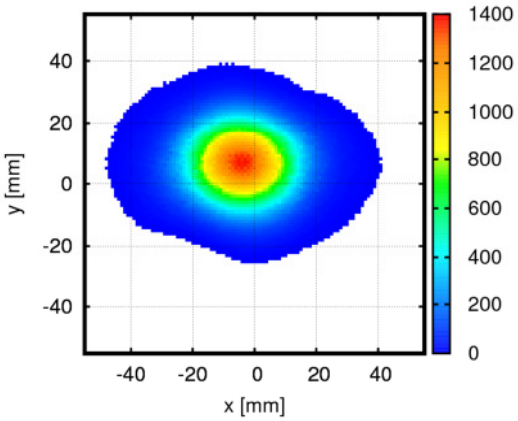

Fig. 19 Measured intensity for vertical polarization

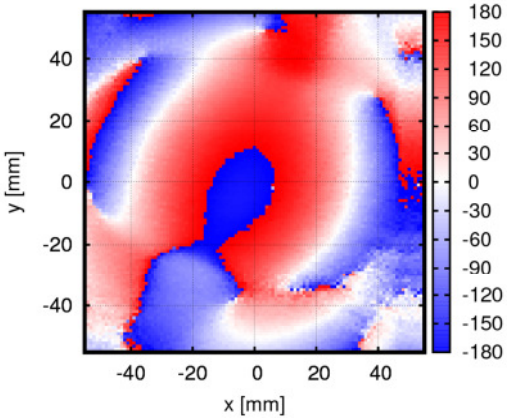

Fig. 20 Measured phase for vertical polarization

Conclusions and outlook

The optimization framework for specialized ECRH reflectors was reworked and improved. It is robust and can use an arbitrary number of computing nodes for the actual optimization with negligible overhead. The resulting surfaces have no discontinuities. The principal reflection characteristics as well as the polarization independence could be verified experimentally.

The parameters needed for the optimizer are in generic reflector-local coordinates, which makes it usable for other experiments as well. The base shape of the mirror can be flat or saddle-type. It is, however, trivial to add other shapes. For W7-X for example, a convex shape might be advantageous.

The described reflector is already coated with tungsten and built into ASDEX-Upgrade. It will be tested with high power during the next experimental campaign.

References

1. H. Höhnle, J. Stober, A. Herrmann, W. Kasparek, F. Leuterer, F. Monaco, R. Neu, D. Schmid-Lorch, H. Schütz, J. Schweinzer, U. Stroth, D. Wagner, S. Vorbrugg, E. Wolfrum and the ASDEX Upgrade Team, *Nucl. Fusion*, **51**, 083013 (2011)
2. E. Poli, A. Bock, M. Lochbrunner, O. Maj, M. Reich, A. Snicker, A. Stegmeir, F. Volpe, N. Bertelli, R. Bilato, G.D. Conway, D. Farina, F. Felici, L. Figini, R. Fischer, C. Galperti, T. Happel, Y.R. Lin-Liu, N.B. Marushchenko, U. Mszanowski, F.M. Poli, J. Stober, E. Westerhof, R. Zille, A.G. Peeters, G.V. Pereverzev, Comp. Phys. Comm., **225**, 36-46, (2018)
3. M. Schubert et.al *This conference* (2018)
4. O. Mangold, *Effiziente holographische Gitterspiegel für die Elektronzyklotronresonanzheizung von Fusionsplasmen*, Doctoral Thesis, Universität Stuttgart, 2009
5. D. Wagner, J. Stober, F. Leuterer, F. Monaco, S. Müller, M. Münich, C. J. Rapson, M. Reich, M. Schubert, H. Schütz, W. Treutterer, H. Zohm, M. Thumm, T. Scherer, A. Meier, G. Gantenbein, J. Jelonnek, W. Kasparek, C. Lechte, B. Plaum, T. Goodman, A.G. Litvak, G.G. Denisov, A. Chirkov, V. Zapevalov, V. Malygin, L.G. Popov, V. O. Nichiporenko, V. E. Myasnikov, E. M. Tai, E.A. Solyanova, S.A. Malygin, ASDEX Upgrade Team, *Journal of Infrared, Millimeter, and Terahertz Waves*, **37**, 45-54 (2016)